Seasonally Evolving Dominant Interannual Variability Modes of East Asian Climate*

BO WU

LASG, Institute of Atmospheric Physics, Chinese Academy of Sciences, and Graduate University of the Chinese Academy of Sciences, Beijing, China

TIANJUN ZHOU

LASG, Institute of Atmospheric Physics, Chinese Academy of Sciences, Beijing, China

TIM LI

IPRC, and Department of Meteorology, University of Hawaii at Manoa, Honolulu, Hawaii

(Manuscript received 7 July 2008, in final form 20 November 2008)

ABSTRACT

A season-reliant empirical orthogonal function (S-EOF) analysis is applied to seasonal mean precipitation over East Asia for the period of 1979–2004. The first two dominant modes account for 44% of the total interannual variance, corresponding to post-ENSO and ENSO turnabout years, respectively. The first mode indicates that in El Niño decaying summer, an anomalous anticyclone appears over the western North Pacific (WNP). This anticyclone is associated with strong positive precipitation anomalies from central China to southern Japan. In the following fall, enhanced convection appears over the WNP as a result of the underlying warm SST anomalies caused by the increase of the shortwave radiative flux in the preceding summer. A dry condition appears over southeastern China. The anomalous precipitation pattern persists throughout the subsequent winter and spring. The second mode shows that during the El Niño developing summer the anomalous heating over the equatorial central Pacific forces a cyclonic vorticity over the WNP. This strengthens the WNP monsoon. Meanwhile, an anomalous anticyclone develops in the northern Indian Ocean and moves eastward to the South China Sea and the WNP in the subsequent fall and winter. This leads to the increase of precipitation over southeastern China. The anticyclone and precipitation anomalies are maintained in the following spring through local air–sea interactions.

The diagnosis of upper-level velocity potential and midlevel vertical motion fields reveals a season-dependent Indian Ocean forcing scenario. The Indian Ocean basinwide warming during the El Niño mature winter and the subsequent spring does not have a significant impact on anomalous circulation in the WNP, because convection over the tropical Indian Ocean is suppressed by the remote forcing from the equatorial central-eastern Pacific. The basinwide warming plays an active role in impacting the WNP anomalous anticyclone during the ENSO decaying summer through atmospheric Kelvin waves or Hadley circulation.

1. Introduction

The East Asian monsoon (EAM) is an important component of the Asian–Australian monsoon (A–AM) system. EAM covers both the tropical and subtropical regions (Zhu et al. 1986), which makes it distinct from the tropical Indian and Australian monsoons. The evolution of EAM exhibits complicated spatial and temporal structures in seasonal cycle (e.g., Tao and Chen 1987; Ding 1992, 1994), interannual variability (e.g., Chang et al. 2000a,b; Zhou and Yu 2005), and interdecadal variability (e.g., Hu 1997; Hu et al. 2003; Yu et al. 2004; Yu and Zhou 2007). The El Niño–Southern Oscillation (ENSO) has been regarded as a major factor modulating the interannual variability of EAM (e.g., Huang and Wu 1989; Chang et al. 2000a,b; Lau and Weng 2001). For example, Huang and Wu (1989), using

* School of Ocean and Earth Science and Technology Contribution Number 7668 and International Pacific Research Center Contribution Number 601.

Corresponding author address: Dr. Tianjun Zhou, LASG, Institute of Atmospheric Physics, Chinese Academy of Sciences, Beijing 100029, China.
E-mail: zhoutj@lasg.iap.ac.cn

DOI: 10.1175/2008JCLI2710.1

data covering 1950–80, found a sandwich precipitation pattern in an ENSO developing summer, with the Yangtze River and Huaihe River Valleys being wet and both North and South China experiencing drought. The most significant precipitation variability along the Yangtze River Valley appears in the Meiyu season after an ENSO peak phase for the period of 1951–99 (Chang et al. 2000a). Wang et al. (2000) proposed a Pacific–East Asia teleconnection mechanism through which ENSO has a delayed impact on EAM. The positive air–sea feedback maintains an anomalous anticyclone and cold SST anomalies (SSTAs) from the El Niño mature winter to early summer in the western North Pacific (WNP). During the summer, the anomalous anticyclone increases precipitation over central China by strengthening the western Pacific subtropical high and shifting it westward (Chang et al. 2000a; Sui et al. 2007; Wu and Zhou 2008). The initial triggering of the anomalous anticyclone may be caused by 1) remote forcing from the tropical central-eastern Pacific SSTA (Wang et al. 2000; Lau and Nath 2000), 2) midlatitude forcing from the north (Wang and Zhang 2002), 3) the eastward displacement of a low-level anomalous anticyclone over the Indian Ocean (IO) (Chou 2004; Chen et al. 2007), or 4) an in-phase transition from a strong Australian monsoon to a strong WNP monsoon associated with a tropospheric biennial oscillation (TBO) cycle (Li et al. 2006).

The EAM has distinctive characteristics relative to the other components of A–AM. The most prominent circulation feature associated with A–AM is two off-equatorial anomalous anticyclones, the South Indian Ocean (SIO) and WNP anticyclones, which have distinctive seasonal-evolution characteristics (Wang et al. 2003). This mode mainly explains the variability over the vast tropical Indo-Pacific Ocean and only accounts for a small percentage of the total variance over the EAM region (see Fig. 6 of Wang et al. 2008). So the issue regarding the dominant modes of the interannual variability of the EAM remains an open problem. In addition, most previous studies on EAM focused on the summertime and little attention has been paid to other seasons. Recent studies revealed coherent variations of EAM during spring and summer at interdecadal time scales (e.g., Li et al. 2005; Xin et al. 2006; Yu and Zhou 2007). Whether there exists coherent variation among different seasons at interannual scales remains unknown. The objective of the present study is to reveal the distinctive seasonal-evolution characteristics of the interannual variation of the EAM. In particular, we attempt to address the following questions: 1) What are the dominant seasonally evolving patterns of the EAM interannual precipitation variability? 2) What are major processes that affect the precipitation variability in the region? 3) How does ENSO remotely affect EAM during its developing and decaying summers? By addressing these issues, we hope to capture the major processes that govern the EAM interannual variability and to provide valuable references for regional climate prediction. Our results indicate that the interannual variability of East Asian precipitation is featured by two seasonally evolving dominant modes, which account for 44% of total variance and correspond to the postdecay phase and turnabout of ENSO, respectively. Remote forcings from equatorial central-eastern Pacific, tropical IO, and local air–sea interaction operate either separately or together during the different phases of ENSO.

The rest of the paper is organized as follows. Section 2 describes the datasets and analyses methods used in present study. Section 3 illustrates the dominant precipitation evolution patterns over the EAM domain. Section 4 describes the circulation and SST patterns associated with the precipitation variability. Section 5 discusses the possible processes through which the IO SSTA remotely impacts the WNP circulation. Finally, a summary is given in section 6.

2. Analysis method and data

Although the conventional empirical orthogonal function (EOF) analysis depicts the spatial pattern and temporal evolution of dominant modes, it cannot obtain coherent seasonal evolution. A season-reliant EOF (S-EOF) analysis was developed to obtain the season-dependent dominant interannual variability modes over the Indo-Pacific domain (e.g., Wang et al. 2003; Wang and An 2005; Li et al. 2006). Here we use the same method but apply it to the EAM domain (15°–45°N, 105°–140°E). Following the concept of a ''monsoon year'' (Yasunari 1991), four seasons, spanning from June–August (JJA) in year 0 [JJA(0)] to March–May (MAM) the following year [year 1; MAM(1)], are linked together. The anomalous fields in the four consecutive seasons are treated as an integral block to construct a covariance matrix. After the EOF decomposition is performed, the yearly block is then divided into four consecutive seasonal anomalies so that a principal component (PC) is derived for each eigenvector that contains a set of seasonally evolving patterns of the anomaly fields from JJA(0) to MAM(1). Note that years 0 and 1 refer to the different temporal phase of S-EOF modes but not to ENSO life cycle. Without specification, spatial patterns described and shown in the paper, as well as associated background fields, correspond to the positive phase of PC.

The interannual variance presents large spatial difference, especially in the EAM region. To clarify that the results obtained from anomalous data do not magnify

contributions from regions with large variability, we have also performed a similar analysis, except with normalized data. The spatial patterns closely resemble those directly derived from the anomalous data (figures not shown). Correlation coefficients of their eigenvectors reach 0.92 (0.73) for the first (second) mode. The PCs are also highly correlated with those derived from the data without normalization, with a correlation coefficient of 0.98 (0.80) for the first (second) mode.

The observational precipitation field derived from the Climate Prediction Center (CPC) Merged Analysis of Precipitation (CMAP) (Xie and Arkin 1997) for the period of 1979–2004 was used in the S-EOF analysis. The other variables include circulation fields from the National Centers for Environment Prediction–National Center for Atmospheric Research (NCEP–NCAR) reanalysis (Kalnay et al. 1996) for the period of 1979–2004; SST fields from the Hadley Centre Sea Ice and Sea Surface Temperature dataset (HadISST) (Rayner et al. 2003) for the period 1978–2005; and flux data for global oceans from the Objectively Analyzed Air–Sea Fluxes (OAFlux) project (Yu et al. 2008) for the period of 1984–2002. Because our focus is the interannual variability of the EAM, prior to S-EOF analysis, variations longer than 8 yr were filtered out from the original datasets with a Lanczos filter (Duchon 1979).

3. Dominant seasonally evolving precipitation patterns

The first two leading modes account for 28.9% and 14.9% of the total variance, respectively. According to the rule of North et al. (1982), the two modes are well distinguished from each other and from the remaining modes. In the following, we explore the distinctive evolution characteristics of large-scale precipitation and circulation fields associated with the two dominant modes.

The seasonally evolving spatial patterns of the first mode are primarily characterized by an evolution of a meridional dipole structure in precipitation anomalies (Fig. 1a). In JJA(0), the dipole pattern appears in the EAM domain, with an elongated band of positive precipitation anomalies extending from the middle and lower reaches of the Yangtze River and Huaihe River Valleys to southern Japan and negative precipitation anomalies over the South China Sea (SCS) and WNP.

The features outside the mainland and those of other seasons are not noted in previous studies. In September–November of year 0 [SON(0)], the precipitation anomalies change their signs, with negative (positive) precipitation anomalies over China and Korea (SCS and WNP). The anomalous precipitation pattern persists from SON(0) to December (year 0)–February (year 1) [D(0)JF(1)]. In MAM(1), the anomalous rainbands shift northward about 10° in latitude and as a result, the southeastern China is dominated by positive precipitation anomalies.

The precipitation evolution pattern of the second mode shows a zonal dipole pattern along 20°N in JJA(0), with positive (negative) precipitation anomalies over the southeastern China (SCS and WNP). In SON(0), the negative precipitation anomalies over the SCS intensify while the positive precipitation anomalies over the southeastern China weaken. Both the negative and positive precipitation anomalies shift eastward in D(0)JF(1) and become stationary afterward.

The depiction of the seasonal evolution is the most distinctive trait of the S-EOF analysis relative to conventional EOF, which is generally used to obtain the dominant modes of the summer monsoon. However, we note that the JJA precipitation anomaly pattern over continental China in the first S-EOF mode resembles that based on EOF analysis of JJA precipitation by using station data (Nitta and Hu 1996; Zhou and Yu 2005), though both the time period and the spatial coverage of the data used in the analysis are different. The resemblance indicates that the dominant mode of East Asian summer monsoon is robust and stable. On the contrary, the second modes of S-EOF and EOF are different: the former is characterized by an anomalous precipitation center over southeastern China, but the latter shows a tripole pattern with coherent variation over North and South China and opposite variation along the Yellow River Valley (Nitta and Hu 1996; Zhou and Yu 2005).

Although the combination of the two dominant modes accounts for about 44% of the total variance, the fractional variances explained by the two modes vary remarkably with location and season. For each field, the variance fraction is defined as the ratio of the variance associated with an S-EOF mode to the corresponding total variance. The spatial and seasonal distributions of the fractional variances for the two modes are shown in Fig. 2. A prominent feature for the first mode is that the largest fractional variance occurs in JJA(0) in the WNP, the SCS, and the middle and lower reaches of the Yangtze River Valley, where the accounted variance exceeds 60%. For the second mode, the maximum variance appears in MAM(1) over eastern China and western Japan. The regions with the maximum variance are associated with significant precipitation anomalies. In addition, relatively large variations are found in D(0)JF(1) in the middle and lower reaches of the Yangtze River Valley for the first mode and in southeastern China for the second mode. Previous studies on A–AM by Wang et al. (2003, 2008) covered a much larger domain (including the entire A–AM and tropical Indo–western-Pacific oceanic region); the derived dominant modes mainly explain a large

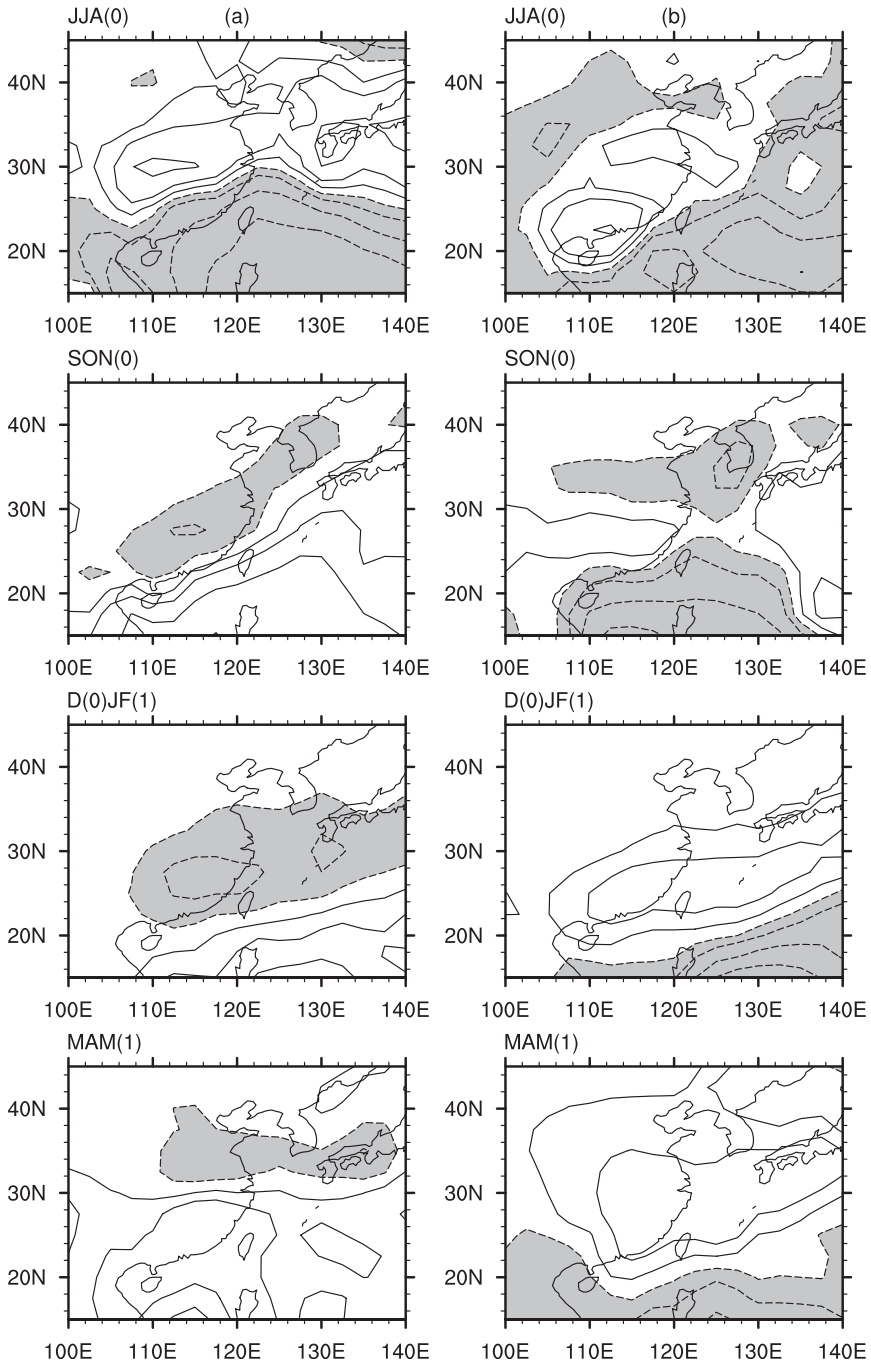

FIG. 1. (a) Seasonally evolving patterns of the first S-EOF mode derived from the CMAP precipitation anomalies over East Asia monsoon domain (mm day^{-1}). (b) Same as (a) except for the second S-EOF mode. Contour values are ±0.1, ±0.3, ±0.7, and ±1.3. Negative values are shaded.

portion of variances over the tropical oceans. Repeating the analysis of Wang et al. (2008) but focusing on the same period of current study, we find that the variance contribution of the first leading modes of the A–AM over the EAM is less than 15% (figures not shown), which is significantly smaller than that of the current study (28.9%). The leading modes revealed in this study show more specific characteristics of the seasonally evolving precipitation anomalies over the EAM land region and explain a much larger portion of variances over the land area.

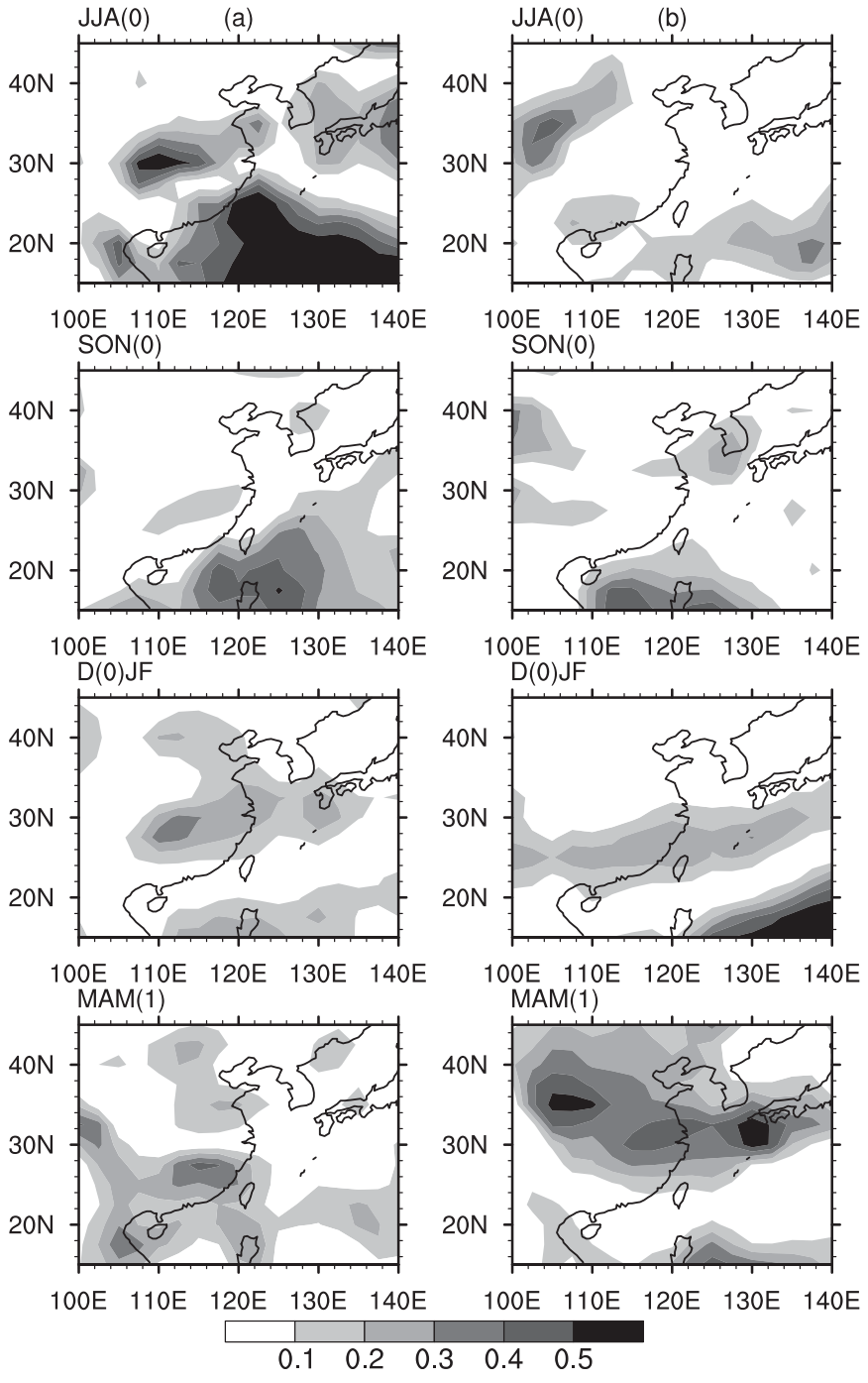

FIG. 2. Fractional variances of the seasonal CMAP precipitation accounted by the (a) first and (b) second S-EOF modes. Contour interval is 10%.

4. Atmospheric circulation and SST patterns associated with the dominant modes of EAM precipitation variability

The lead–lag correlations of the first PC (PC1) with the area-averaged SSTA over the Niño-3.4 (5°S–5°N, 120°–170°W) and topical IO (10°S–10°N, 40°–110°E) regions are shown in Fig. 3a. Here year (−1) [year (1)] denotes that Niño-3.4 leads (lags) the PC1 time series by one year. Note that the PC1 is positively correlated with the Niño-3.4 index in year (−1), with the correlation coefficient exceeding 0.5 and passing the threshold of

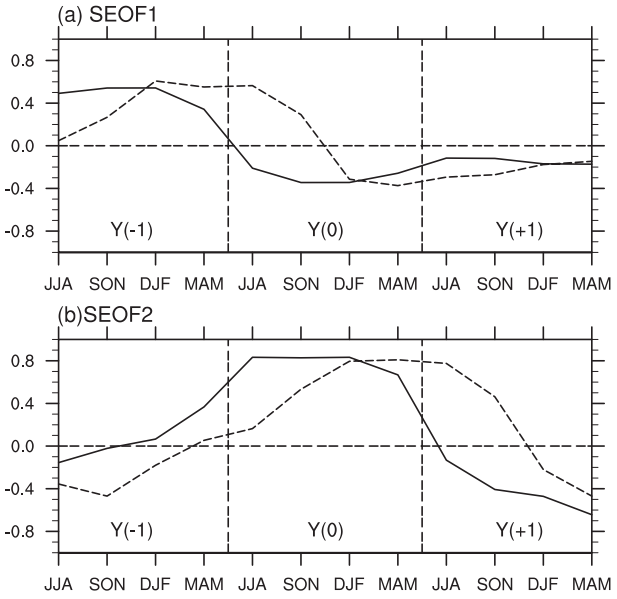

FIG. 3. (a) Lead–lag correlations between the first S-EOF principal component and the Niño-3.4 index (solid line) and the Indian Ocean basinwide warming index (dashed line). The Indian Ocean basinwide warming index is defined as area-averaged SSTAs in the tropical Indian Ocean (10°S–10°N, 40°–110°E). (b) As in (a), but for the second mode.

the 5% significance level. However, the simultaneous correlation between them is not statistically significant at the 5% level. This indicates that the first mode occurs following the peak of the ENSO event. The significant simultaneous correlation between PC1 and the IO SSTA index in JJA(0) suggests that the basinwide IO SSTA plays a crucial role in prolonging the impact of ENSO on the EAM during the ENSO decaying summer.

The lead–lag correlation between the second PC (PC2) and the Niño-3.4 index shows a significant simultaneous correlation (larger than 0.8), indicating that the second mode is primarily associated with the development and turnabout of ENSO (Fig. 3b). Thus, the two S-EOF modes reflect the dominant seasonally evolving patterns during the post-ENSO and ENSO turnabout years, respectively. Meanwhile, the lead–lag correlation between PC2 and the IO SST index reaches the peak phase from DJF(0) to JJA(1), lagging the highest correlation between PC2 and Niño-3.4 index by two seasons. It is consistent with Fig. 3a and suggests that the IO prolongs the impact of ENSO on the EAM.

Wu et al. (2003) investigated the relationship between season-evolving variability of EAM and ENSO through extended singular value decomposition (E-SVD). The dominant mode derived from the E-SVD primarily accounts for EAM in ENSO developing and mature phases (see their Fig. 6). However, in our study, the first dominant mode corresponds to the year after a peak ENSO episode and the second mode corresponds to ENSO turnabout. The differences of the dominant modes of S-EOF and E-SVD may come from the foothold of two analysis methods: the former focuses on the self-evolution of EAM, whereas the latter primarily depicts the linkage between EAM and ENSO. The difference also suggests that many factors, in addition to ENSO, contribute to the variance of EAM.

The seasonally evolving atmospheric circulation and SST patterns associated with the first mode are shown in Fig. 4. Here the 850-hPa wind, 500-hPa vertical pressure velocity, and SST anomalies are regressed upon the PC1 time series. To show its evolution associated with the mature phase of ENSO, we show the figures from two seasons prior to JJA(0). During the El Niño mature phase D(−1)JF(0), two prominent off-equatorial anomalous anticyclones appear over the SIO and WNP. Although the SIO anticyclone is a direct Rossby wave response to suppressed convection over the Maritime Continent (Wang et al. 2003), the WNP anticyclone is fully coupled with underlying cold water through a positive thermodynamic air–sea feedback (Wang et al. 2000, 2003). A basinwide warming occurs in the tropical IO. The suppressed convection over the eastern IO (Fig. 4a) implies that the local SSTA warming is the result of atmospheric forcing (Klein et al. 1999). The convection over the eastern IO and Maritime Continent is dominated by the equatorial central-eastern Pacific through anomalous Walker circulation but not IO local passive warm SST. Therefore, IO local SSTAs cannot exert a remote forcing to the WNP during the El Niño mature winter.

In MAM(0), the WNP anomalous anticyclone persists because of positive feedback from the local cold SSTA. Over the tropical IO, as the maximum warm SSTA appears south to the equator, an equatorial asymmetric mode develops, with 500-hPa ascending (descending) motion anomalies appearing over the south (north) of the equator and low-level cross-equator southward wind converging toward the tropical SIO (Wu et al. 2008). Because the El Niño-induced subsidence still dominates the Maritime Continent, the IO basinwide warming has little impact on the WNP anticyclone in MAM(0).

A remarkable feature appears in the vertical motion in JJA(0), namely a basinwide ascending branch occurs in the tropical IO, even though the amplitude of the IO SSTA is weaker than the SSTAs in the preceding winter and spring. This basinwide (including the Maritime Continent) convective heating anomaly may have a significant impact on the WNP circulation in the El Niño decaying summer. To further illustrate the possible IO impact, we plot 200-hPa velocity potential anomalies and corresponding divergent wind fields for the first mode in Fig. 5.

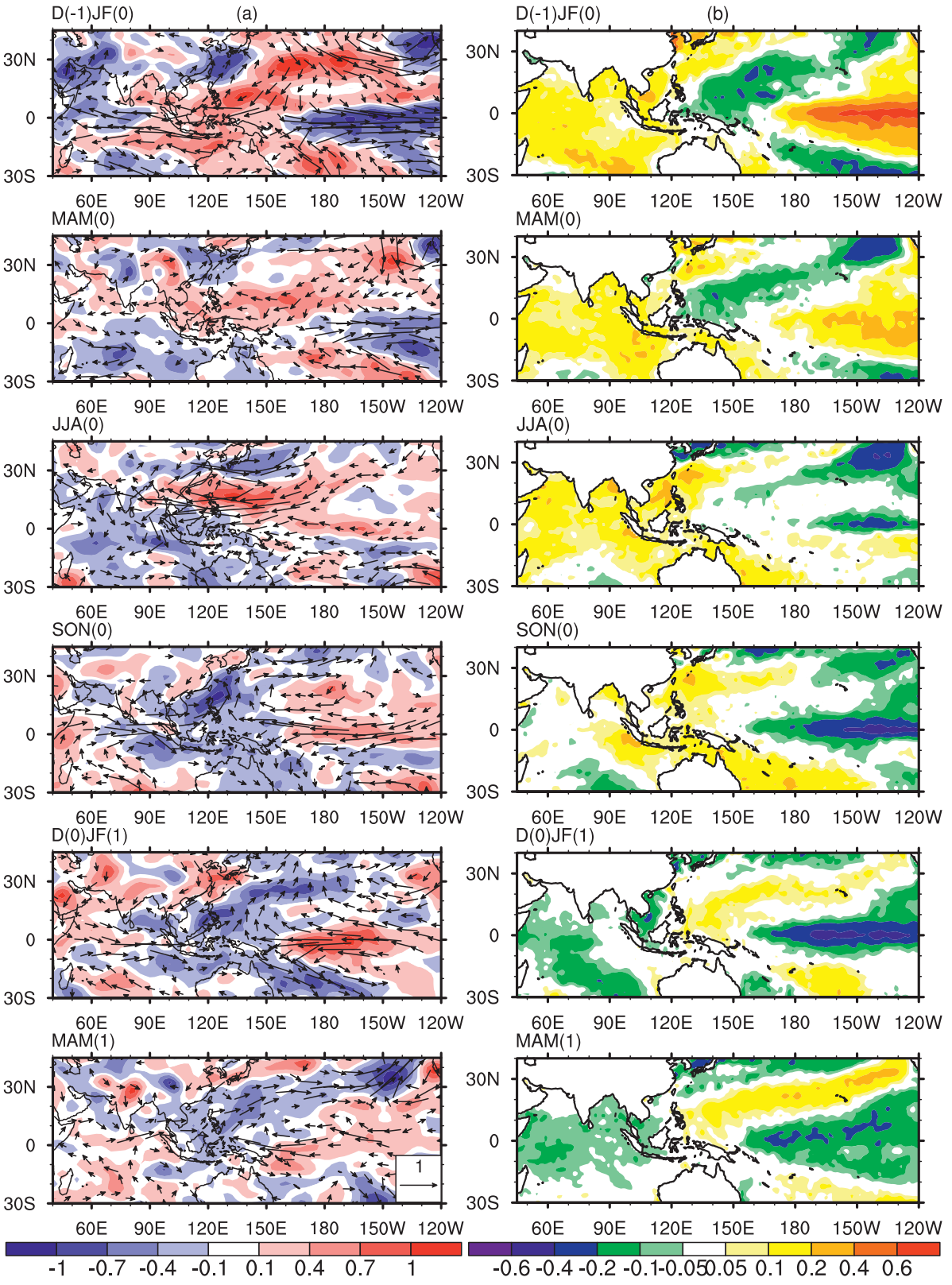

FIG. 4. Seasonally evolving patterns of (a) 850-hPa wind (m s^{-1}; vector) and 500-hPa vertical p-velocity (shaded, 10^{-2} hPa s^{-1}) anomalies regressed onto the principal component of the first S-EOF mode. (b) The corresponding seasonal mean SSTAs (K).

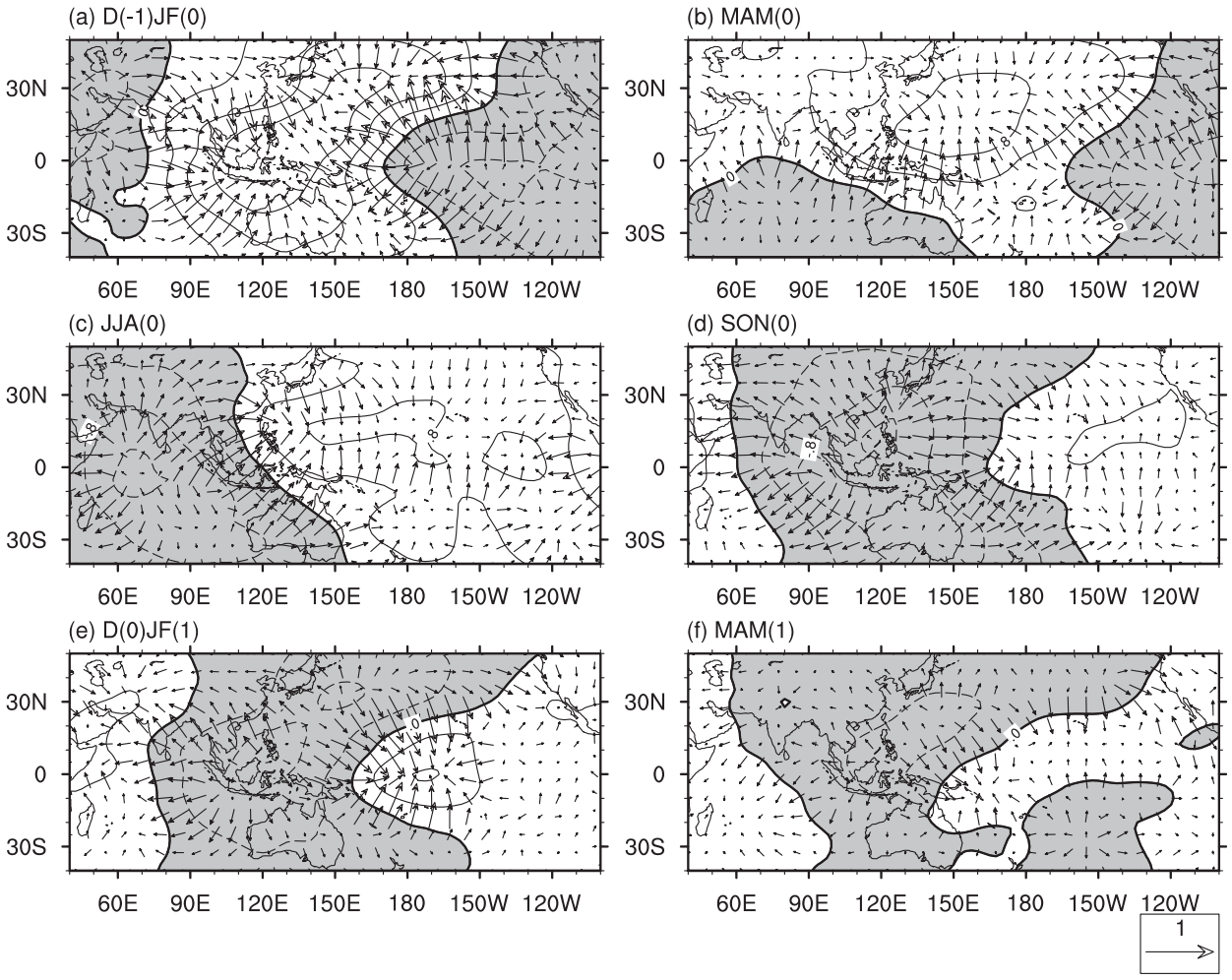

FIG. 5. Same as Fig. 4a, except for 200-hPa velocity potential (contours, 10^{-6} m^2 s^{-1}, interval 0.4, negative values shaded); and divergent wind (vectors, m s^{-1}).

In D(−1)JF(0), the upper-level convergences over the WNP, Maritime Continent, and tropical eastern IO are primarily connected to strong divergences over the tropical central-eastern Pacific associated with El Niño forcing. Only a weak divergent center appears over the far western IO. In MAM(0), the upper-level divergence over the IO, primarily located to the south of the equator, is much weaker than that over the tropical eastern Pacific. The entire Maritime Continent and WNP are controlled by the upper-level convergence, which is consistent with 500-hPa subsidence anomalies. Thus, the WNP anticyclones in both seasons are maintained by remote SSTA forcing from the tropical central-eastern Pacific and the local wind–evaporation–SST feedback (Wang et al. 2000), whereas the tropical IO SSTA plays a minor role. In JJA(0), following the rapid decay of El Niño, the upper-level divergence completely disappears in the eastern Pacific, whereas the tropical IO is fully occupied by a strong upper-level divergent center. It is only during this season that the IO SSTA is likely to be able to exert a significant impact on the WNP circulation.

The southerly anomalies to the western boundary of the anomalous anticyclone may transport more water vapor to central China (Chang et al. 2000a), leading to an increase of precipitation extending from the middle and lower reaches of the Yangtze River and Huaihe River Valleys to southern Japan. Over the SCS and WNP, the anomalous anticyclone causes a dry condition. Therefore, the precipitation anomaly in JJA(0) exhibits a meridional dipole pattern (Fig. 1a). The precipitation dipole pattern closely resembles part of the negative phase of the classical Pacific–Japan (PJ) pattern (Nitta 1987; Huang and Sun 1992; Nitta and Hu 1996; Kosaka and Nakamura 2006). A well-organized north–south wavelike pattern along the East Asian coast is seen in the 850-hPa vorticity of the S-EOF 1 JJA(0) (figure not shown).

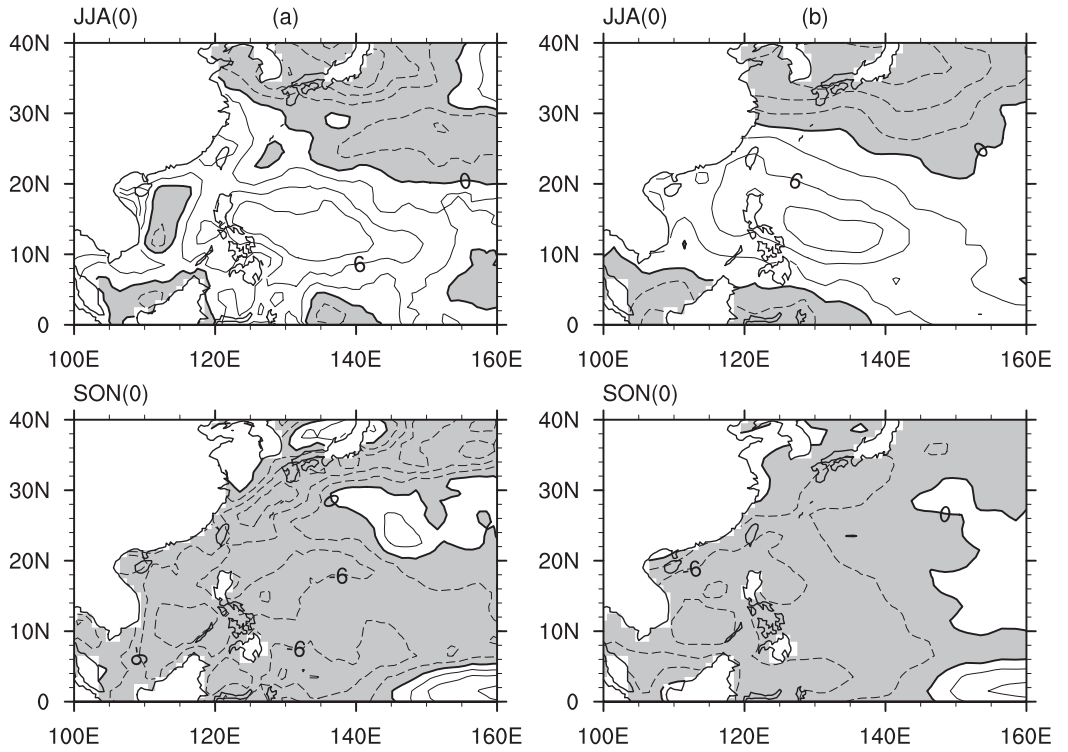

FIG. 6. (a) Net surface heat flux and (b) shortwave radiative flux anomalies (W m^{-2}) in (top) JJA(0) and (bottom) SON(0) regressed onto the principal component of the first S-EOF mode. The net surface heat flux consists of the shortwave radiation, longwave radiation, latent heat flux, and sensible heat flux derived from the OAFlux dataset. Positive values are downward. Contour interval is 3 and negative values are shaded.

In JJA(0), as the mean flow changes to pronounced southwesterly flows over the WNP, the positive air–sea feedback that appears in the preceding winter and spring is no longer valid. Rather, a negative wind–evaporation–SST feedback leads to the decay of cold SSTAs in the WNP (Wang et al. 2003). Meanwhile, the suppressed convection associated with the anomalous anticyclone causes a decrease of clouds and an increase of downward shortwave radiative flux. A comparison of heat fluxes indicates that the shortwave radiative flux has a major contribution to the net heat flux anomalies (which consist of shortwave radiation, longwave radiation, latent heat flux, and sensible heat flux components) in JJA(0) (Fig. 6). The positive net heat flux anomalies lead to the warmer SSTA in the region.

In SON(0), the WNP anomalous anticyclone shifts eastward associated with the development of a La Niña episode. As the seasonal maximum convection moves southeastward from India to the SCS (Meehl 1987), the local positive SSTA that persisted from the preceding season enhances the convection and stimulates an anomalous cyclone over the SCS (Fig. 4a). This leads to a change of sign of precipitation anomalies over the SCS from negative in JJA(0) to positive in SON(0). Meanwhile, the northerly winds to the west of the cyclone transport dry and cold air from higher latitudes, leading to a dry condition in southeastern China (Fig. 1a).

The enhanced convection over the SCS damps the local positive SSTA in SON(0) by reducing shortwave radiative fluxes (see Fig. 6). In D(0)JF(1), the enhanced convection and anomalous cyclone move eastward. An anomalous subsidence prevails to the northwest of the cyclone, leading to a decrease of precipitation over southeastern China and southern Japan. The anomalous cyclone persists from D(0)JF(1) to MAM(1), as positive SSTAs develop to the east of the Philippines (Fig. 4b).

The seasonally evolving 850-hPa wind, 500-hPa vertical pressure velocity, and SST anomalies for the second S-EOF mode are shown in Fig. 7. This mode starts from ENSO developing summer and ends after the mature phase of ENSO. The seasonal evolution of SSTA exhibits a typical El Niño life cycle, with a rapid development in JJA(0) and SON(0), a peak in D(0)JF(1), and a decay in MAM(1) (Rasmusson and Carpenter 1983).

In JJA(0), the warm water in the equatorial central-eastern Pacific enhances the local convection. In response to this anomalous heating, strong westerly anomalies over the equator and a pair of anomalous cyclones over the

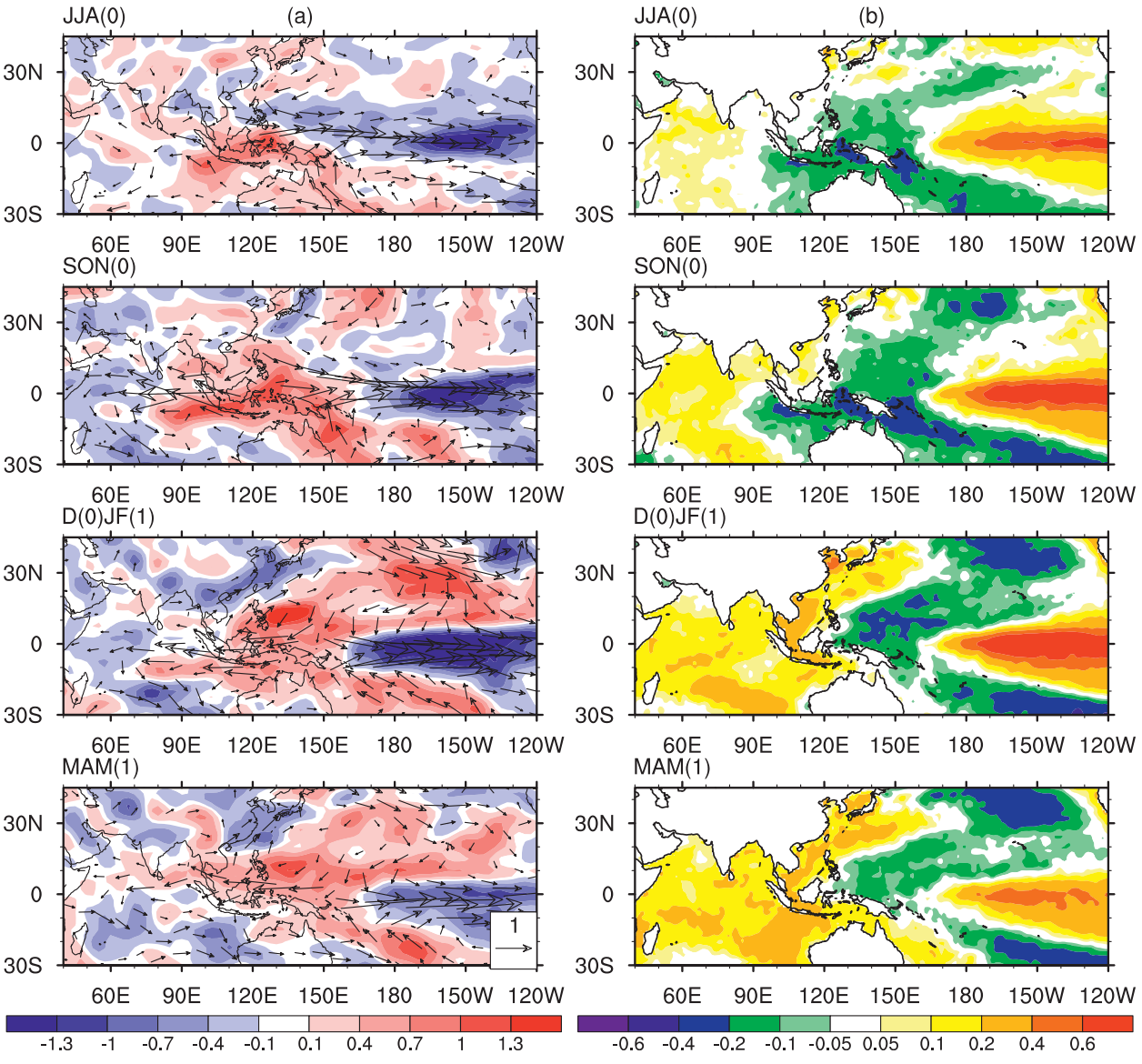

FIG. 7. As in Fig. 4, but for the second S-EOF mode.

western Pacific are generated according to the classical Matsuno–Gill pattern (Matsuno 1966; Gill 1980). The anomalous cyclones are most intense over the WNP (0–15°N, 125–160°E) because of the mean flow asymmetry. These cyclones intensify the WNP summer monsoon. Meanwhile, an anomalous low-level anticyclone forms over the northern IO and moves eastward to the SCS/WNP. The eastward propagation is attributed to an east–west asymmetry, relative to the anticyclone center, of the divergent flow and moisture fields (Chou 2004; Chen et al. 2007). As a result, the convection is suppressed over the SCS and the Philippine Sea from SON(0) to MAM(1).

The anomalous anticyclone is maintained during the turnabout of El Niño through the aforementioned positive air–sea feedback (Wang et al. 2000, 2003). The anomalous southerly to the west of the anticyclone transports more water vapor northward and finally results in an excessive precipitation belt extending from southeastern China to southern Japan, which is the most significant precipitation anomaly during the ENSO mature phase [D(0)JF(1) and MAM(1)] over East Asia.

For the second mode, the IO SSTA experiences a remarkable change from the IO dipole or zonal mode (Saji et al. 1999; Webster et al. 1999) in JJA(0) and SON(0) to a basinwide warming in D(0)JF(1) and MAM(1) (Fig. 7b). Previous studies suggested that the warming of the eastern IO can be caused either by an increase of solar fluxes associated with remote El Niño

forcing (Klein et al. 1999; Lau and Nath 2003; Venzke et al. 2000) or by ocean wave dynamics (Li et al. 2003). As shown above, the IO basinwide warming may play a primary role in affecting the WNP circulation during the ENSO decaying summer.

5. Possible impacts of IO basinwide warming on the WNP circulation: A discussion

Previous studies suggested that the WNP anticyclone persists from winter to early summer through both the local wind–evaporation–SST feedback and the El Niño remote forcing (Wang et al. 2000; Lau and Nath 2000). In boreal summer, with the shift of the basic-state wind from northeasterly to southwesterly over the WNP, the air–sea feedback changes from positive to negative. Meanwhile, the SSTA in the equatorial central-eastern Pacific decays. Why does the WNP anticyclone still strengthen in the summer? First, although the negative SSTA in the WNP established in the preceding DJF and MAM completely disappears in JJA (Fig. 4), the dissipation of negative SSTA is a gradual process. Significant cold SSTAs prior to monsoon onset may weaken the WNP monsoon strength, leading to anomalous anticyclonic flows in situ. Second, the IO SSTA may prolong the influence of ENSO by exerting a direct impact on the WNP monsoon during the ENSO decaying summer (see discussions in section 4). It is consistent with the capacitor mechanism that El Niño extends its impact to EAM through forcing IO warming (Yang et al. 2007). Two questions remain open. First, through what processes does the IO SSTA have a remote impact on the WNP circulation? Second, what are the relative roles of the IO basinwide warming and the local negative SSTA in the WNP prior to the monsoon onset in causing the anomalous WNP anticyclone in the El Niño decaying summer?

Although the IO basinwide warming can persist from El Niño mature winter to decaying summer, it only exerts a significant impact on the WNP anticyclone in the summer. In El Niño mature winter and the following spring, the warm SSTAs in the equatorial central-eastern Pacific stimulate strong anomalous Walker circulation, the downwelling branch of which suppresses convection over the IO (Klein et al. 1999). In contrast to the condition of preceding winter and spring, intensive ascending motion occupies the entire tropical IO in the El Niño decaying summer (Fig. 4a), even though the basinwide warming may not be as strong as that in the preceding seasons. Correspondingly, the upper-tropospheric velocity potential field is characterized by a dipole pattern with strong divergences over the IO and convergences over the WNP (Fig. 5). This implies that it is only in the El Niño decaying summer that the eastern IO and Maritime Continent are completely out of the control of remote El Niño forcing and thus able to force the atmosphere freely. This season-dependent IO SSTA forcing provides a memory for prolonging the impact of El Niño on the WNP anticyclone.

Two possible mechanisms are hypothesized through which the IO basinwide warming may affect the WNP anticyclone. First, the basinwide convective heating of the IO in JJA forces anomalous low-level easterlies over the tropical western Pacific as a Kelvin wave response, according to the classical Matsuno–Gill solution (Matsuno 1966; Gill 1980). The easterlies have the maximum amplitude on the equator and decrease with latitude. The anticyclonic shear of the easterly anomalies induces a divergence in the atmospheric planetary boundary layer (PBL) resulting from the Ekman pumping process. The subsidence at the top of the PBL and the divergence in the PBL lead to the decrease of local-specific humidity and moist static energy, which weakens the WNP monsoon convection. The suppressed heating further locally induces an anomalous anticyclone. A schematic view of the possible mechanism is presented in Fig. 8.

Second, the persistent basinwide warming of the IO leads to the increase of the surface moisture resulting from enhanced surface evaporation. In boreal summer, climatological westerlies are pronounced along the equatorial IO. The average westerly transports more moisture into the Maritime Continent, thereby causing enhanced convection over the continent (Fig. 4a). The strengthened convective heating over the Maritime Continent may induce a local Hadley circulation and cause the anomalous subsidence over the WNP, which in turn forces a local anomalous anticyclone. This mechanism was first proposed by Hu (1997) to interpret the impact of the IO on the interdecadal change of summer climate in China. It was later used to explain the low-frequency interannual oscillation of the western Pacific subtropical high in observational analysis (Sui et al. 2007) and modeling studies (Wu and Zhou 2008).

It is important to note that although either the Kelvin wave response or the anomalous Hadley circulation is symmetric about the equator in a resting environment in response to a symmetric IO SSTA forcing, the asymmetry of the summer mean state favors a much greater response north of the equator because the maximum seasonal convective heating is located along the monsoon trough at about 15°N. The mean state is crucial in determining the preferred location of the WNP anticyclone.

Although the IO basinwide warming has been established in the mature phase of El Niño (boreal winter), it does not affect the WNP circulation because the SSTA at the eastern IO is a passive response to atmospheric

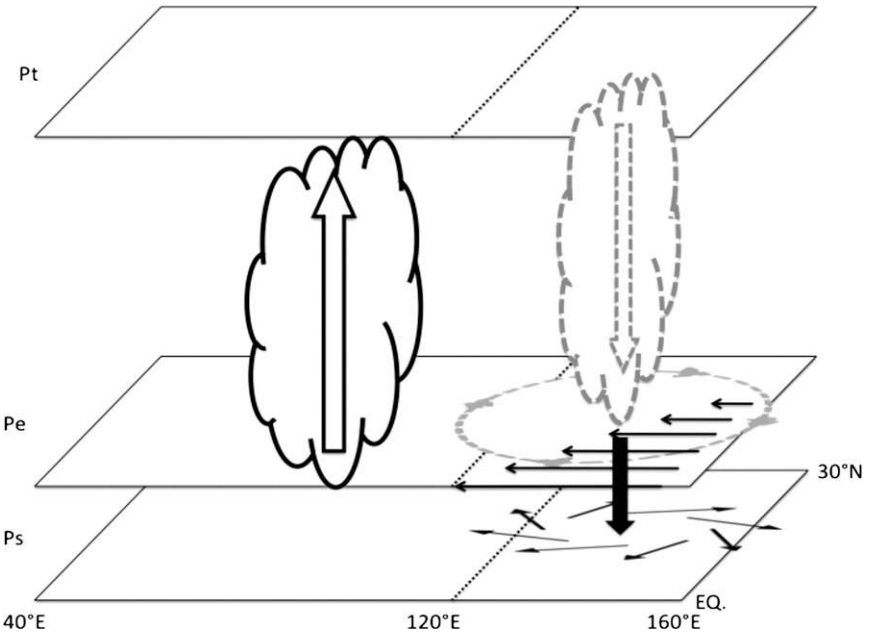

FIG. 8. Schematic diagram illustrating how the tropical IO heating influences the WNP monsoon during the El Niño decaying summer. Pressure at the surface, the top of the planetary boundary layer, and the top of the troposphere are denoted by Ps, Pe, and Pt, respectively. In response to the enhanced convection over the tropical IO, easterly wind anomalies (solid black arrowheads on Pe) are established as an atmospheric Kelvin wave response to the anomalous heating. The anomalous anticyclonic shear vorticity induces the anomalous subsidence (thick black arrowheads) resulting from the Ekman pumping effect and thus the boundary layer divergence (solid black arrowheads between Pe and Ps). The anomalous boundary layer divergence further leads to suppressed convection (dashed curve and hollow arrowhead) and a low-level anomalous anticyclone (dashed circle) over the WNP.

forcing (a negative SST–precipitation relationship). During boreal winter and subsequent seasons, the WNP anomalous anticyclone is maintained by local cold SSTAs through a positive thermodynamic air–sea feedback (Wang et al. 2003). As seen in Fig. 4b, by the end of spring [MAM(0)], significant cold SSTAs appear in the WNP. Although, after the monsoon onset, the mean southwesterly in the region would lead to a negative air–sea feedback and thus reduce the amplitude of SSTA, the significant negative SSTAs prior to monsoon onset may exert a strong impact on the WNP monsoon. Thus, both the local cold SSTA and the IO basinwide warming may contribute to the WNP anomalous anticyclone in the El Niño decaying summer.

6. Summary and concluding remarks

Based on a season-reliant EOF analysis, we have revealed two dominant modes of the seasonally evolving interannual variability modes of the EAM and their relationships with ENSO and IO basinwide warming. The first mode corresponds to the year after a peak ENSO episode and the second mode corresponds to the ENSO developing and turnabout phases. The evolutions of large-scale circulation and SST patterns associated with the two modes are further documented. Below we summarize the major seasonal-evolution characteristics of the EAM modes in terms of the ENSO phases.

1) In the El Niño developing summer, warm SSTAs in the equatorial central-eastern Pacific influence the East Asian monsoon through enhancing convection over the WNP. Meanwhile, an anomalous anticyclone forms over the northern IO, which moves eastward to the SCS in the subsequent fall. During the El Niño peak winter and the following spring, the anomalous anticyclone is located over the WNP, which interacts with the underlying SST. While negative precipitation anomalies appear over the WNP, positive precipitation anomalies develop from southeastern China to southern Japan. Meanwhile, a basinwide warming appears in the tropical IO.
2) In the El Niño decaying summer, negative SSTAs in the WNP gradually dissipate because of a negative air–sea feedback, but the anomalous anticyclone still maintains and is even stronger than that in spring.

The precipitation along the middle and lower reaches of the Yangtze River and Huaihe River Valleys is greatly enhanced as a result of the enhanced moisture transport by anomalous southerlies from the western flank of the anomalous anticyclone. From the upper-level velocity potential field, the anomalous subsidence in the WNP is closely related to the convective activity associated with the IO basin warming. The subsidence over the WNP makes the local SST warm through increased shortwave radiative fluxes. In the subsequent fall, with the decay of basinwide warm SSTA in the IO, the anticyclone over the WNP cannot be maintained; instead, the local warm SSTA enhances the convection over the SCS, leading to an enhanced precipitation over the SCS. In the following winter and spring, the anomalous cyclone shifts slightly to the Philippine Sea and is maintained through its interaction with a warm SSTA belt in the WNP. The anomalous circulation pattern leads to a negative rain belt extending from southeastern China to Japan.

3) With the decay of the equatorial-central–eastern-Pacific SSTA and the seasonal variation of the climate mean wind during the El Niño decaying summer, both the remote forcing and local air–sea feedback cannot maintain the anomalous WNP anticyclone. The IO basinwide warming is an essential external forcing to maintain the WNP anticyclone in the summer. The effect of IO basin warming is seasonally dependent and only plays an active role in the ENSO decaying summer.
4) The IO basinwide warming suppresses convection over the WNP and thereby strengthens the WNP anticyclone through two processes. First, the basinwide warming enhances the local convection, which stimulates a Kelvin wave–type low-level easterly response over the tropical western Pacific. The anticyclonic shear vorticity associated with the easterly response leads to Ekman pumping–induced boundary layer divergences, which may weaken the WNP monsoon through reducing the moist static energy. Second, the IO basinwide warming leads to enhanced convection over the Maritime Continent, which further induces anomalous subsidence over the WNP through anomalous Hadley circulation.

For the future work of this study, as discussed in the previous section, both the cold SSTA in the WNP prior to the monsoon season and the positive SSTA in the tropical IO during the monsoon season may have significant impacts on the summertime WNP anticyclone. Their relative roles, however, remain to be clarified. This warrants further studies from both observational analyses and idealized numerical experiments.

In addition, because reliable global precipitation datasets are only available from 1979, our analysis is based on data covering 26 yr (1979–2004), which may not be long enough to investigate the impact of different ENSO phases on East Asian climate. There are similar problems for the results of Huang and Wu (1989), which used 1950–80 data to make the composites. That may also be one of the reasons why the theory of Huang and Wu (1989) was not successful in the operational climate prediction. Although the current results need to be verified in the future by using longer datasets, the outputs of long-term simulations of coupled climate models may help us to understand the impact of sample size.

Acknowledgments. This work was supported by NSFC Grants 40628006, 40625014, and 40675050 and the National Basic Research Program of China (2006CB403603). TL was also supported by ONR Grants N000140710145, N00173061G031, and N000140810256 and by the International Pacific Research Center, which is sponsored by the Japan Agency for Marine-Earth Science and Technology (JAMSTEC), NASA (NNX07AG53G), and NOAA (NA17RJ1230).

REFERENCES

Chang, C. P., Y. S. Zhang, and T. Li, 2000a: Interannual and interdecadal variations of the East Asian summer monsoon and tropical Pacific SSTs. Part I: Roles of the subtropical ridge. *J. Climate,* **13,** 4310–4325.

——, ——, and ——, 2000b: Interannual and interdecadal variations of the East Asian summer monsoon and tropical Pacific SSTs. Part II: Meridional structure of the monsoon. *J. Climate,* **13,** 4326–4340.

Chen, J. M., T. Li, and C. F. Shih, 2007: Fall persistence barrier of sea surface temperature in the South China Sea associated with ENSO. *J. Climate,* **20,** 158–172.

Chou, C., 2004: Establishment of the low-level wind anomalies over the western North Pacific during ENSO development. *J. Climate,* **17,** 2195–2212.

Ding, Y. H., 1992: Summer monsoon rainfall in China. *J. Meteor. Soc. Japan,* **70,** 373–396.

——, 1994: *Monsoons over China.* Kluwer Academic, 420 pp.

Duchon, C. E., 1979: Lanczos filtering in one and two dimensions. *J. Appl. Meteor.,* **18,** 1016–1022.

Gill, A. E., 1980: Some simple solutions for heat-induced tropical circulation. *Quart. J. Roy. Meteor. Soc.,* **106,** 447–462.

Hu, Z., 1997: Interdecadal variability of summer climate over East Asia and its association with 500-hPa height and global sea surface temperature. *J. Geophys. Res.,* **102,** 19 403–19 412.

——, S. Yang, and R. Wu, 2003: Long-term climate variations in China and global warming signals. *J. Geophys. Res.,* **108,** 4614, doi:10.1029/2003JD003651.

Huang, R., and Y. Wu, 1989: The influence of ENSO on the summer climate change in China and its mechanism. *Adv. Atmos. Sci.,* **6,** 21–32.

——, and F. Sun, 1992: Impacts of the tropical western Pacific on the East Asian summer monsoon. *J. Meteor. Soc. Japan,* **70,** 243–256.

Kalnay, E., and Coauthors, 1996: The NCEP/NCAR 40-Year Reanalysis Project. *Bull. Amer. Meteor. Soc.,* **77,** 437–471.

Klein, S. A., B. J. Soden, and N. C. Lau, 1999: Remote sea surface temperature variations during ENSO: Evidence for a tropical atmospheric bridge. *J. Climate,* **12,** 917–932.

Kosaka, Y., and H. Nakamura, 2006: Structure and dynamics of the summertime Pacific-Japan teleconnection pattern. *Quart. J. Roy. Meteor. Soc.,* **132,** 2009–2030.

Lau, K.-M., and H. Weng, 2001: Coherent modes of global SST and summer rainfall over China: An assessment of the regional impacts of the 1997–98 El Niño. *J. Climate,* **14,** 1294–1308.

Lau, N.-C., and M. J. Nath, 2000: Impact of ENSO on the variability of the Asian–Australian monsoons as simulated in GCM experiments. *J. Climate,* **13,** 4287–4309.

——, and ——, 2003: Atmosphere–ocean variations in the Indo-Pacific sector during ENSO episodes. *J. Climate,* **16,** 3–20.

Li, J., R. Yu, T. Zhou, and B. Wang, 2005: Why is there an early spring cooling shift downstream of the Tibetan Plateau? *J. Climate,* **18,** 4660–4668.

Li, T., B. Wang, C.-P. Chang, and Y. Zhang, 2003: A theory for the Indian Ocean dipole–zonal mode. *J. Atmos. Sci.,* **60,** 2119–2135.

——, P. Liu, X. Fu, B. Wang, and G. A. Meehl, 2006: Spatiotemporal structures and mechanisms of the tropospheric biennial oscillation in the Indo-Pacific warm ocean regions. *J. Climate,* **19,** 3070–3087.

Matsuno, T., 1966: Quasi-geostrophic motions in the equatorial area. *J. Meteor. Soc. Japan,* **44,** 25–42.

Meehl, G. A., 1987: The annual cycle and interannual variability in the tropical Pacific and Indian Ocean region. *Mon. Wea. Rev.,* **115,** 27–50.

Nitta, T., 1987: Convection activities in the tropical western Pacific and their impact on the Northern Hemisphere summer circulation. *J. Meteor. Soc. Japan,* **65,** 375–383.

——, and Z.-Z. Hu, 1996: Summer climate variability in China and its association with 500-hPa height and tropical convection. *J. Meteor. Soc. Japan,* **74,** 425–445.

North, G. R., T. L. Bell, R. F. Cahalan, and F. J. Moeng, 1982: Sampling errors in the estimation of empirical orthogonal functions. *Mon. Wea. Rev.,* **110,** 699–706.

Rasmusson, E. M., and T. H. Carpenter, 1983: Variations in tropical sea surface temperature and surface wind fields associated with the Southern Oscillation/El Niño. *Mon. Wea. Rev.,* **111,** 517–528.

Rayner, N. A., D. E. Parker, E. B. Horton, C. K. Folland, L. V. Alexander, D. P. Rowell, E. C. Kent, and A. Kaplan, 2003: Global analyses of sea surface temperature, sea ice, and night marine air temperature since the late nineteenth century. *J. Geophys. Res.,* **108,** 4407, doi:10.1029/2002JD002670.

Saji, N. H., B. N. Goswami, P. N. Vinayachandran, and T. Yamagata, 1999: A dipole mode in the tropical Indian Ocean. *Nature,* **401,** 360–363.

Sui, C.-H., P.-H. Chung, and T. Li, 2007: Interannual and interdecadal variability of the summertime western North Pacific subtropical high. *Geophys. Res. Lett.,* **34,** L11701, doi:10.1029/2006GL029204.

Tao, S. Y., and L. X. Chen, 1987: A review of recent research of the East Asian summer monsoon in China. *Monsoon Meteorology,* C.-P. Chang and T. N. Krishnamurti, Eds., Clarendon, 60–92.

Venzke, S., M. Latif, and A. Villwock, 2000: The coupled GCM ECHO-2. Part II: Indian Ocean response to ENSO. *J. Climate,* **13,** 1371–1383.

Wang, B., and Q. Zhang, 2002: Pacific–East Asian teleconnection. Part II: How the Philippine Sea anomalous anticyclone is established during El Niño development. *J. Climate,* **15,** 3252–3265.

——, and S.-I. An, 2005: A method for detecting season-dependent modes of climate variability: S-EOF analysis. *Geophys. Res. Lett.,* **32,** L15710, doi:10.1029/2005GL022709.

——, R. G. Wu, and X. H. Fu, 2000: Pacific–East Asian teleconnection: How does ENSO affect East Asian climate? *J. Climate,* **13,** 1517–1536.

——, ——, and T. Li, 2003: Atmosphere–warm ocean interaction and its impacts on Asian–Australian monsoon variation. *J. Climate,* **16,** 1195–1211.

——, J. Yang, T. Zhou, and B. Wang, 2008: Interdecadal changes in the major modes of Asian–Australian monsoon variability: Strengthening relationship with ENSO since the late 1970s. *J. Climate,* **21,** 1771–1789.

Webster, P. J., A. M. Moore, J. P. Loschnigg, and R. R. Leben, 1999: Coupled ocean-temperature dynamics in the Indian Ocean during 1997-98. *Nature,* **401,** 356–360.

Wu, B., and T. Zhou, 2008: Oceanic origin of the interannual and interdecadal variability of the summertime western Pacific subtropical high. *Geophys. Res. Lett.,* **35,** L13701, doi:10.1029/2008GL034584.

Wu, R., Z.-Z. Hu, and B. P. Kirtman, 2003: Evolution of ENSO-related rainfall anomalies in East Asia. *J. Climate,* **16,** 3742–3758.

——, B. P. Kirtman, and V. Krishnamurthy, 2008: An asymmetric mode of tropical Indian Ocean rainfall variability in boreal spring. *J. Geophys. Res.,* **113,** D05104, doi:10.1029/2007JD009316.

Xie, P., and P. A. Arkin, 1997: Global precipitation: A 17-year monthly analysis based on gauge observation, satellite estimate, and numerical model outputs. *Bull. Amer. Meteor. Soc.,* **78,** 2539–2558.

Xin, X., R. Yu, T. Zhou, and B. Wang, 2006: Drought in late spring of South China in recent decades. *J. Climate,* **19,** 3197–3206.

Yang, J., Q. Liu, S.-P. Xie, Z. Liu, and L. Wu, 2007: Impact of the Indian Ocean SST basin mode on the Asian summer monsoon. *Geophys. Res. Lett.,* **34,** L02708, doi:10.1029/2006GL028571.

Yasunari, T., 1991: The monsoon year—A new concept of the climatic year in the tropics. *Bull. Amer. Meteor. Soc.,* **72,** 1331–1338.

Yu, L., X. Jin, and R. A. Weller, 2008: Multidecade global flux datasets from the Objectively Analyzed Air–Sea Fluxes (OAFlux) Project: Latent and sensible heat fluxes, ocean evaporation, and related surface meteorological variables. Woods Hole Oceanographic Institution OAFlux Project Tech. Rep. OA-2008-01, 64 pp.

Yu, R., and T. Zhou, 2007: Seasonality and three-dimensional structure of the interdecadal change in the East Asian monsoon. *J. Climate,* **20,** 5344–5355.

——, B. Wang, and T. Zhou, 2004: Tropospheric cooling and summer monsoon weakening trend over East Asia. *Geophys. Res. Lett.,* **31,** L22212, doi:10.1029/2004GL021270.

Zhou, T.-J., and R.-C. Yu, 2005: Atmospheric water vapor transport associated with typical anomalous summer rainfall patterns in China. *J. Geophys. Res.,* **110,** D08104, doi:10.1029/2004JD005413.

Zhu, Q., J. He, and P. Wang, 1986: A study of circulation differences between East-Asian and Indian summer monsoons with their interaction. *Adv. Atmos. Sci.,* **3,** 466–477.